This paper appears in IEEE/ASME Transactions on Mechatronics.
https://doi.org/10.1109/TMECH.2020.2981625

Using Potential Field Function with a Velocity Field Controller to Learn and Reproduce the Therapist's Assistance in Robot-Assisted Rehabilitation

Mohammad Najafi, Carlos Rossa, Kim Adams, and Mahdi Tavakoli

Abstract— **Rehabilitative and assistive practices usually elicit intense and repetitive exercises. Thus, there has been an increasing interest in robotic systems as they are robust and cost-effective in comparison to conventional physical motor-therapy with a therapist. These robots have applications in therapeutic and in-home environments, where there is a necessity for a user-friendly procedure to program the robots for a specific task easily. Our group has suggested robot learning from demonstration (LfD) as an intuitive procedure to program robots via short-term physical interaction in rehabilitation and assistive applications. In this paper, a therapist assists a patient, and cooperatively performs a task on a robotic manipulator. Then, using a non-parametric potential field function, the therapist's motion and interaction force (assistance/resistance) is modelled time-independently via a convex optimization algorithm. Next, in the therapist's absence, the robot provides the patient with the same level of interaction force provided by the therapist along the trajectory. A velocity field controller is also designed to compensate and regulate the patient's deviation from the velocity observed in the demonstration phase. Finally, the efficacy, advantages, and stability of the proposed framework are evaluated in three different experimental scenarios involving spring arrays and an individual with Cerebral Palsy.**

I. Introduction

Stroke and cerebral palsy are the most common causes of severe movement disorders in adults and children, respectively [1]. Symptoms associated with these disorders include loss of motor control, reduced mobility, restricted range of motion, muscle stiffness, and difficulties in performing a voluntary movement. It is estimated that about 460,000 Canadians are living with the effects of stroke [2], and more than 500,000 Americans under the age of 18 have at least one cerebral palsy symptom that negatively affects their daily life tasks [3]. Due to the ageing population in Canada and the growing population in the USA, the need for therapeutic and rehabilitative services is expected to increase in the near future [2], [4].

The proposed system in this paper can be useful in various applications that involves human-robot interaction. However, without the loss of generality, this work is focused on providing arm-reaching motor-therapy to individuals with an upper-limb disability. There are various approaches to entirely or partially restore the physical functionality of stroke patients and ameliorate motor function in individuals with CP [5], [6]. However, conventional arm-reaching practices are labor intensive and constitute a significant load for therapists as they involve high-dose intensive training and repetitive practices of specific functional tasks [6], [7]. As an alternative in recent years, there has been an increasing interest in bringing robotic systems into the clinical scene to assist individuals with task executions [5]. This, however, emphasizes on a critical issue: 1) The field of robotics is dynamic and evolving, but, there has been no proof that an intelligent robotic system can prescribe therapeutic or assisting motions and replicate an expert therapist [7], 2) when interacting with humans, robots must be able to be robust and deal with uncertainties while performing a given task and classical robot position control falls short in addressing this issue since it works time-dependently with no feedback from the patient.

To control both robot's motion and dynamics at points of contact with its surrounding environment, variable impedance control has been widely used in collaborative robotics to regulate the interaction between the human and the robotic manipulator. It allows adaption of robot interaction properties, for instance, by making it more or less compliant in uncertain regions, while cooperatively accomplishing a task such as following a given path [8]. Variable impedance control requires real-time motion generation to operate jointly with the controller. To this end, robot learning from demonstration (LfD) can be considered. LfD is a technique for creating trajectories that rely on demonstrations of an intended task to a robotic manipulator. LfD algorithms use a dataset of examples to reproduce the demonstrated behavior [9].

LfD has initially been developed for industrial settings (see [10] for a survey). In our previous works, we demonstrated that LfD could also be efficiently used along with impedance controllers in the context of rehabilitation to use the therapist's demonstrated therapy task to program the robotic manipulator for repetitive high-intensity reproduction of the task with the patient [11]–[14]. In this scenario, the therapist performed the task of moving an initially inert robotic manipulator from point A to point B for multiple times. This was referred to as the "demonstration phase."

This research was supported by the Canada Foundation for Innovation (CFI) under grant LOF 28241, the Alberta Innovation and Advanced Education Ministry under Small Equipment Grant RCP-12-021, the Natural Sciences and Engineering Research Council (NSERC) of Canada under a Collaborative Health Research Projects (CHRP) Grant, the Canadian Institutes of Health Research (CIHR), and Quanser, Inc.

M. Najafi, C. Rossa, and M. Tavakoli are with the Department of Electrical and Computer Engineering, University of Alberta, AB, Canada. E-mail: najafi@ualberta.ca; carlos.rossa@uoit.ca; mahdi.tavakoli@ualberta.ca.

K. Adams is with the Faculty of Rehabilitation Medicine at the University of Alberta, and the Glenrose Rehabilitation Hospital, Edmonton, AB, Canada. E-mail: kdadams@ualberta.ca.

Then the system learned the task-specific trajectory provided by the therapist. Next, in the therapist's absence, the robot assisted the patient with following the same trajectory. This was referred to as the "robot-assistance phase." A virtual impedance model (a spring-damper pair in parallel) attracted the robot manipulator to the learned trajectory. Thus, if the patient deviates from the demonstrated trajectory at a given time, assistance is provided to prevent further deviation from the trajectory, at a rate that is proportional to the observed deviation.

The previous LfD approach in our group used Gaussian mixture models (GMM) to mathematically capture the trajectory followed by the therapist and patient. Gaussian mixture regression (GMR) was employed to reproduce the demonstrated trajectory using robotic assistance.

There are ways to improve upon the previous approach. First, it should be noted that the assistance provided by LfD algorithms in the traditional way are time-dependent [12]. Thus, the patient is required to follow the demonstrated trajectory from the initial position towards the destination at a similar velocity as in the demonstration phase. Otherwise, the patient would experience interaction forces programmed for other sections of the trajectory (as it is time-indexed) and the robot increases the applied force uncontrollably to drag the user's hand to the desired path, with no feedback from the patient's success in following the trajectory. Second, the demonstration phase did not involve the patient, but only the therapist is demonstrating the desired position (trajectory) and allowed deviation to the robot. This approach fails to capture the required patient-specific interaction force and velocity. Third, to address the system's stability and safety issues of the first two points. In this paper, we further extend the idea of LfD for robotics-assisted rehabilitation to address these three points.

Rather than using traditional LfD algorithms, we propose a framework that uses a modified version of the non-parametric potential field function introduced in [15] for the context of robotic rehabilitation. Readers are referred to [15] if they are interested to know the advantages of this method over other state-of-the-art LfD techniques in-detail. In our proposed framework, first, the therapist and patient cooperatively perform a task for once. Then, the robot motion and interaction forces are captured by a non-parametric potential function's gradient and curvature, respectively, using a convex optimization algorithm. In this paper, the convex optimization target has been modified so that the potential field is shaped based on both tangential and normal (perpendicular to the trajectory) interaction forces between therapist and patient. Then, in the therapist's absence, the robot, controlled by the learned potential field, provides the patient with an estimated assistance and interaction behaviour he/she received during the demonstration phase. Normal gradients keep the patient around the trajectory, and tangential curvature assists the patient in moving along the trajectory.

In [15], there was no human-robot interaction in the reproduction phase. Therefore, a constant dissipating field was calculated by solving a convex optimization to produce

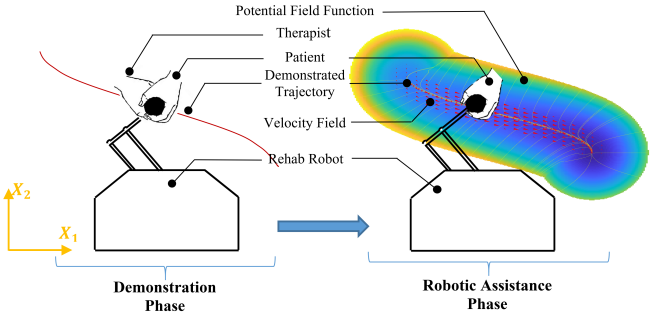

Fig. 1. Displays the proposed framework for learning the therapist's assistance by demonstration. In the demonstration phase (left), the therapist assists the patient to follow the trajectory for a single trial. Then, in the robotic assistance phase (right), by using potential field function and velocity field controller, the demonstrated therapist's assistance is modelled and provided to the patient.

motions with the velocity equal to the demonstrated velocity. However, in this paper, the robot is interacting with a human in the reproduction phase. Therefore, a performance-based velocity field controller is proposed to adapt to the variant user behavior and provide them with assistance/resistance if they are deviating from the demonstrated velocity. A position-indexed velocity field is produced around the trajectory based on the demonstrated velocity. Then, the stable velocity field controller proposed in [16] is used to regulate the patient's deviation from the demonstrated velocity. Finally, the stability of the overall system is proven in interaction with a passive environment. Fig. 1 displays the proposed framework. The remainder of this paper is organized as follows: Section II introduces the cooperative task demonstration phase, subsequently used in Section III in order to derive the modified potential field function. In Section IV, we propose the velocity field controller and prove the stability of the overall system. Finally in Section V, we validate the proposed approach in a 2-dimensional Cartesian space task using a planar rehabilitation robot.

II. Task Demonstration

It is assumed that the patient, if unassisted, is unable to complete a given task. Therefore, the therapist also interacts with the robotic manipulator held by the patient in order to assist him/her to carry out a task, considering the patient's physical constraints and range of motion. The therapist provides the minimum required assistance (i.e., assist-as-needed) to motivate the patient to actively engage in the task [17], [18]. In this framework, just a single demonstration is required for the system to learn the therapist's assistance.

The nonlinear dynamics of a multi degree of freedom (DOF) rigid robot in the n-dimensional Cartesian coordinates can then be given by:

$$M(q_r)\ddot{x}_r + C(q_r,\dot{q}_r)\dot{x}_r + G(q_r) + f(\dot{q}_r) = F_{in} + F_c \quad (1)$$

where $q_r \in \mathbb{R}^{n\times 1}$ are the joint angles, $x_r \in \mathbb{R}^{n\times 1}$ is the position of the robot end effector in the Cartesian coordinates, $M(q_r) \in \mathbb{R}^{n\times n}$ is the inertia matrix, $C(q_r,\dot{q}_r) \in \mathbb{R}^{n\times n}$ contains Coriolis and centrifugal terms, $G(q_r) \in \mathbb{R}^{n\times 1}$ contains

position-based forces such as gravity and $f(q_r) \in \mathbb{R}^{n\times 1}$ is the friction force. Also, F_{in} and $F_c \in \mathbb{R}^{n\times 1}$ are interaction and control forces, respectively, exerted on the robotic end effector. Note that as the robotic manipulator interacts with the task environment, the therapist pulls/pushes the robot to assist the patient to complete the task. It is assumed that the slave robot is either inherently back-drivable or is properly impedance-controlled to follow externally-imposed motions.

With therapist holding the robotic manipulator and end effector in contact with patient, as they cooperatively perform a task, let

$$\begin{aligned} F_{in} &= F_{th} + F_{pa} + F_d \\ F_c &= 0 \end{aligned} \tag{2}$$

in (1), where F_{th}, F_{pa}, and $F_d \in \mathbb{R}^{n\times 1}$ are the placeholders that represent the force applied by therapist, patient and disturbance to the robotic manipulator, respectively. F_{in} is measured by force sensor in the robotic end effector.

A. Data Sampling and Preprocessing

During the demonstration phase, the n-dimensional position $x_P \in \mathbb{R}^n$, velocity $\dot{x}_p \in \mathbb{R}^n$ and interaction force between the therapist and the patient ($F_{in} \in \mathbb{R}^n$) in the Cartesian coordinates are sampled with a constant sampling time. Since the position vector samples are not evenly distributed along the trajectory, as velocity is not constant, the dataset is down-sampled to M evenly-distributed samples (hereafter called attracting points) to form the following dataset:

$$D = \{[x_p^i; \dot{x}_p^i; F_{in}^i \in \mathbb{R}^n] \in \mathbb{R}^{3n}\}_{i=1}^{M} \in \mathbb{R}^{3n\times M} \tag{3}$$

where the superscript i is for the i^{th} attracting point of the demonstrated trajectory, which contains M attracting points in total.

Now, $\{T-N\}^i$, which is the tangential-normal coordinate system in the i^{th} attracting point is defined, which is centered at x_p^i with the tangential axis toward the next attracting point (x_p^{i+1}). T and N represent the tangential and normal direction in this Cartesian coordinates, respectively. The rotation matrix between the $\{T-N\}^i$ and inertial Cartesian coordinate system can be calculated in each attracting point as $R_p^i(\theta_p^i)$. Thereby, F_{in}^i and x_p^i can be represented in $\{T-N\}^i$, with tangential $\{x_{p,T}^i, F_{in,T}^i \in \mathbb{R}\}$ and normal $\{x_{p,N}^i, F_{in,N}^i \in \mathbb{R}^{n-1}\}$ components, through the rotation matrix $R_p^i(\theta_p^i)$ as:

$$\begin{aligned} [\dot{x}_{p,T}^i \;\; \dot{x}_{p,N}^i]^{\mathrm{T}} &= R_p^i(\theta_p^i)\dot{x}_p^i \\ [F_{in,T}^i \;\; F_{in,N}^i]^{\mathrm{T}} &= R_p^i(\theta_p^i)F_{in}^i \end{aligned} \quad \forall i \in \{1,2,...,M\} \tag{4}$$

III. Learning the Potential Field Function

To robotically reproduce therapist's assistance, potential function learning, which was initially proposed in [15] is used. In the reproduction phase, the therapist is not present and the robotic manipulator provides assistance through the control signal $F_c \in \mathbb{R}^{n\times 1}$, such that in (1) we substitute:

$$\begin{aligned} F_{in} &= F_{pa} + F_d \\ F_c &= F_{pot}(x_r) + F_{vel}(x_r, \dot{x}_r) \end{aligned} \tag{5}$$

in which

$$F_{pot}(x_r) = -\nabla U(x_r) \in \mathbb{R}^{n\times 1} \tag{6}$$

is the gradient of the positive scalar potential field at each position ($U(x_r) \in \mathbb{R}^+$) and $F_{vel}(x_r, \dot{x}_r) \in \mathbb{R}^{n\times 1}$ denotes the velocity field controller in the task environment which both will be defined hereafter.

To provide identical assistive forces as demonstrated, to the patient, two fundamental set of forces are required:

1) The attracting force $F_{in,N}^i$, which is normal to the trajectory, attracts the end effector and resists deviations from the trajectory.
2) The propelling force $F_{in,T}^i$, which is tangent to the trajectory and assists the patient to move along the trajectory and reach the destination.

To jointly generate both tangential and normal forces that are applied at a given position, the non-parametric potential field is created by connecting the current position of the end effector x_r to each attracting point x_p^i through a virtual spring model with stiffness K. The calculated potential energy stored in each spring is:

$$u^i(x_r) = u_0^i + \frac{1}{2}(x_r - x_p^i)^T K^i (x_r - x_p^i) \;\; \forall i \in \{1,2,...,M\}, \tag{7}$$

in which $u_0^i \in \mathbb{R}^+$ is the bias potential parameter and $K^i \in \mathbb{R}^n$ is a diagonal stiffness matrix in the i^{th} attracting point. The higher the stiffness matrix, the higher the attracting force $K^i(x_r - x_p^i)$ will be towards the i^{th} attracting point.

In order to smooth out and localize the accumulated potential field produced by all position samples (i.e., attracting points), Gaussian kernel regression is employed. The total potential energy as in [15] through the weighed average will be:

$$U(x_r) = \sum_{i=1}^{M} \widetilde{\omega}^i(x_r) u^i(x_r) \tag{8}$$

with

$$\widetilde{\omega}^i(x_r) = \frac{\omega^i(x_r)}{\sum_{i=1}^{M} \omega^i(x_r)} \tag{9}$$

and

$$\omega^i(x_r) = e^{-\frac{1}{2\sigma_i^2}(x_r - x_p^i)^T (x_r - x_p^i)} \tag{10}$$

where $\sigma^i > 0$ is a smoothing parameter with $0 < \widetilde{\omega}^i(x_r) < 1$, and $\sum_{i=1}^{M} \widetilde{\omega}^i = 1$. As shown in Fig. 2, u_0^i and K^i determine the tangential gradient and normal gradient of the potential field, respectively. In the proposed robotic assistance scenario, the potential field parameters (u_0^i and K^i) are set to represent the interaction of the therapist with the patient during the cooperative task demonstration. To replicate the therapist's normal force along the trajectory, the stiffness matrix K^i is set to be diagonal and linearly proportional to the demonstrated normal interaction force as (11-12). Therefore, the robotic system will assist (i.e., attract) the patient toward the trajectory, as needed. The stiffness matrix is then defined as:

$$K^i = diag[K_T^i \;\; K_{N_1}^i \;\; ... \;\; K_{N_{n-1}}^i] \tag{11}$$

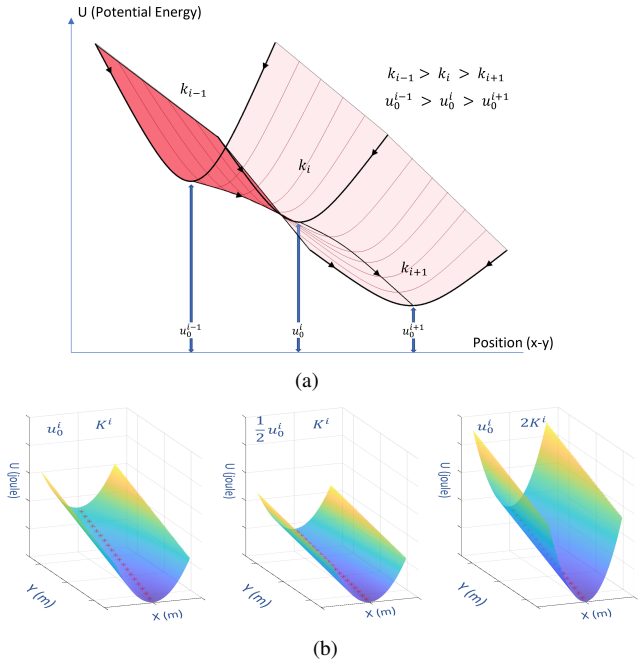

Fig. 2. (a) Displays a section of a potential field function that models a trajectory along i, $i-1$, and $i+1$ attracting points. As attracting points are close to each other along the trajectory, the stiffness parameters (K^{i-1}, K^i, K^{i+1}) have a negligible effect on the tangential gradient, which is mainly dictated by the difference in bias potentials (u_0^{i-1}, u_0^i, u_0^{i+1}). (b) Illustrates the effect of u_0^i and K^i parameters on the potential field gradient (i.e., force) in the tangential and normal directions, respectively.

in which:

$$K_{N_j}^i = \frac{F_{in,N_j}^i - F_{in,N_j,min}}{F_{in,N_j,max} - F_{in,N_j,min}}(K_{N_j,max} - K_{N_j,min}) + K_{N_j,min} \quad \forall j \in \{1,2,...,n-1\} \tag{12}$$

where $F_{in,N_j,max}$ and $F_{in,N_j,min}$ are the maximum and minimum normal interaction force observed in j^{th} normal direction in the demonstration phase. Also, $K_{N_j,max}$ and $K_{N_j,min}$ are the maximum and minimum stiffness parameters in j^{th} normal direction (in 2D tasks $j=1$) tuned based on the task-specific requirements and robot physical restrictions (e.g., actuator torque). In the next step, having the stiffness parameters in each attracting point, calculated using (12), the potential field biases (u_0) can be calculated based on a convex optimization method so that the gradient of the potential field in i^{th} attracting point ($-\nabla u^i(x_p^i,\Theta)$) gets equal to the tangential interaction force observed in the demonstration phase. The optimization minimizes

$$\min_{u_0} \; J(\Theta) = \sum_{i=1}^{n} \|\nabla u^i(x_p^i,\Theta) + {F_{in,T}^i}^+\|_2 \tag{13}$$

subject to:

$$\begin{aligned} &u_0^{i+1} \le u_0^i && \forall i \in \{1,2,...,M-1\} \\ &u_0^i \ge 0 && \forall i = M \\ &\nabla u^i(x_p^i,\Theta) = 0 && \forall i = M \\ &\Theta = \{u^i, k^i\} && \forall i \in \{1,2,...,M-1\} \end{aligned} \tag{14}$$

where M corresponds to the last attracting point (destination) of the demonstrated trajectory. $\nabla u^i(x_p^i,\Theta)$ and ${F_{in,T}^i}^+$ which are gradient of potential field and demonstrated tangential interaction force are also defined as:

$$\nabla u^i(x_p^i,\Theta) = -\sum_{i=1}^{M} \frac{\widetilde{\omega}^i(x_r)}{(\sigma^i)^2}(u(x_p^i) - U(x_p^i)) + .. \\ \widetilde{\omega}^i(x_r)K^i(x_r - x_p^i) \tag{15}$$

and

$${F_{in,T}^i}^+ = \begin{cases} F_{in,T} & \text{if } F_{in,T} >= 0 \\ 0 & \text{otherwise} \end{cases} \tag{16}$$

The convex optimization in (13) finds the optimized bias potential parameter (u_0^i), so the learned potential field dictates the position-related force, same as the therapist's demonstrated interaction force along the trajectory and exerts it on patient's hand via the robotic end effector. Fig. 3. displays the overall framework for learning the potential field.

IV. Velocity Field Controller

During the reproduction phase, the robotic manipulator should follow the trajectory with an acceleration and velocity identical to the demonstration phase. However, variability is inevitable in human motions. In this section, a velocity field controller is defined to adjust the transient response of the system and regulate the patient's velocity around the demonstrated trajectory. In the first step, the desired velocity in each position is calculated by the weighted average of the demonstrated velocity as:

$$\dot{x}_d(x_r) = \Pi_0^L(dis(x_r,x_p)) \sum_{i=1}^{M} \widetilde{\omega}^i(x_r)\dot{x}_p^i \tag{17}$$

where $\dot{x}_d(x_r) \in \mathbb{R}^n$ represents the position-based desired velocity. $\dot{x}_p^i \in \mathbb{R}^n$ denotes the demonstrated velocity in each sample and $\Pi_a^b(x) \in \mathbb{R}^+$ is the smooth transition function that can be chosen from the sigmoid function family as:

$$\Pi_a^b(x) = \frac{1}{2} - \frac{1}{2}tanh\left(\frac{6(x - \frac{a+b}{2})}{b-a}\right) \tag{18}$$

in (17), $L \in \mathbb{R}^+$ denotes the width of the velocity field, and $dis(x_r,x_p) \in \mathbb{R}^+$ expresses the minimum distance of robotic end effector, x_r, from the attracting points, x_p. The smooth transition function is multiplied to restrict the width of the velocity field around the trajectory. The aim is to minimize the interference of the velocity field with the potential field for the asymptotic stability of the accumulated field. In areas away from the trajectory, the potential field gradient (i.e., force) is mainly normal to the trajectory. This normal force pulls the patient toward the trajectory and enhances patient's accuracy in following the trajectory. Therefore, any added velocity field (which is aimed to be followed by the patient) will interfere with this normal force and compromise the asymptotic stability toward the destination position. However, in the vicinity of the trajectory, the potential field gradient is mainly tangential, and the velocity

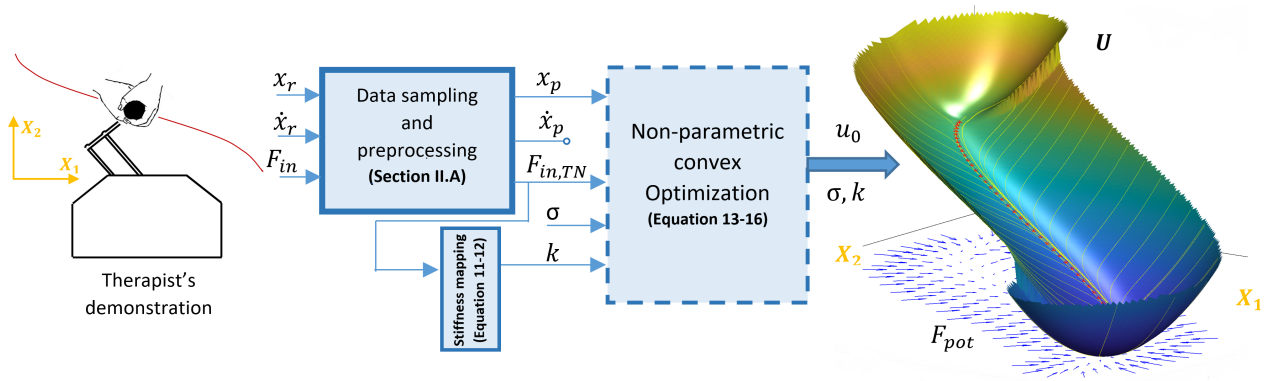

Fig. 3. Illustrates the proposed framework for learning the therapist's assistive interaction force from demonstration, using potential field function in Section III. x_r, $\dot{x}_r$, and F_{in} are recorded during the therapist's assistance demonstration to the patient. Then down-sampled and processed (Section II-A) to be provided to the convex optimization which finds the optimum u_0 in the potential field to replicate the tangential interaction field provided by the therapist (13).

field contributes to asymptotic stability. The potential and velocity field are jointly sketched in Fig. 4.

Now, in order to regulate the robot's velocity, we will use a varying dissipative field controller proposed in [16]. This controller separately regulates the velocity in the tangential direction and selectively dissipates energy in the normal directions to the desired velocity. This is achieved by a full ranked variable damping matrix, whose orthogonal eigenvectors rotate based on the desired velocity direction ($\widehat{v_T} = \frac{\dot{x}_d(x_r)}{||\dot{x}_d(x_r)||}$) and span the task space as:

$$D(x_r) = Q(x_r)\ C\ Q(x_r)^T \tag{19}$$

$$Q(x_r) = [\widehat{v_T}\ \ \widehat{v_{N_1}}\ \ ...\widehat{v_{N_n}}] \tag{20}$$

$$C = diag\ [c_T\ \ c_{N_1}\ \ ...c_{N_{n-1}}] \tag{21}$$

In (19), $D(x_r)$ denotes the position-based varying damping matrix and $Q(x_r)$ represents the eigenvector matrix that transforms diagonal eigenvalue matrix (C) to inertial Cartesian coordinates. In (20), $\widehat{v_T}$ represents the normalized tangential direction vector, and $\{\widehat{v_{N_1}},...,\widehat{v_{N_n}}\}$ are the normalized arbitrary and orthogonal vectors normal to the desired velocity. The eigenvalues c_T and $\{c_{N_1},...,c_{N_n}\}$ in (21) represent the tunable damping parameters in tangential and normal directions to the desired velocity, respectively. Having the variable damping matrix, the velocity field controller in (5) is:

$$F_{vel}(x_r,\dot{x}_r) = -D(x_r)(\dot{x}_r - \gamma(Z,S)\dot{x}_d(x_r)) = \\ -D(x_r)\dot{x}_r + \gamma(Z,S)c_T\dot{x}_d(x_r) \tag{22}$$

where $\dot{x}_d(x_r)$ is an eigenvector of $D(x_r)$, with corresponding eigenvalue c_T. Therefore, $D(x_r)\dot{x}_d(x_r) = c_T\dot{x}_d(x_r)$ in (22) with $\gamma(Z,S) \in \mathbb{R}^+$ being the stabilizing energy tank scalar function which is discussed in the following paragraphs. The velocity field controller damps the motion normal to the desired velocity (tuned by $\{c_{N_1},...,c_{N_n}\}$), while regulating the velocity tangent to the desired velocity $\dot{x}_d(x_r)$. If the patient is following the trajectory slower than the desired velocity, the controller will actively push (assist) the patient to go faster. On the other hand, if the patient is going faster than the desired velocity, the controller resists and dissipates energy. The tangent velocity deviation tolerance can be tuned by the therapist through tangential damping parameter c_T.

The velocity field controller with its variable position-based damping matrix, $D(x_r)$, can insert energy into the system, thereby compromising stability. As suggested in [16], the energy tank is employed to ensure the non-passivity of the system. Energy tank refers to an additive state that stores the dissipative energy of the system (instead of wasting it), and uses this stored energy to induce it back to the system when active control action is required. Therefore, the energy tank state $S \in \mathbb{R}$ which has a rate of change ($\dot{S}$) defined as:

$$\dot{S} = \alpha(S)\dot{x}(x_r)D(x_r)\dot{x}(x_r) - \beta(Z,S)c_T Z \tag{23}$$

in which $Z = \dot{x}(x_r)^T\dot{x}(x_d)$ and

$$\alpha(S) = \begin{cases} 1 & \text{if } S < \bar{S} \\ 0 & \text{otherwise} \end{cases} \tag{24}$$

and,

$$\beta(Z,S) = \begin{cases} 0 & \text{if } S \le 0\ \&\ Z \ge 0 \\ 0 & \text{if } S \ge \bar{S}\ \&\ Z \le 0 \\ 1 & \text{otherwise} \end{cases} \tag{25}$$

where the $\dot{S}$ represents the rate in which the energy tank is charging (positive rate) or depleting (negative rate). The term $\dot{x}(x_r)D(x_r)\dot{x}(x_r) \in \mathbb{R}^+$ is always positive as the damping matrix, $D(x_r)$, is positive definite. This is the dissipated passive energy that charges the energy tank and is controlled by a scalar multiplier $\alpha(S)$. $\alpha(S)$ is set to zero if the tank reaches its maximum energy level, ($\bar{S}$), as in (24). In (23), $Z = \dot{x}(x_r)^T\dot{x}(x_d)$ indicates the tangential velocity tracking that is either active ($Z > 0$) or passive ($Z < 0$). The $\beta(Z,S)$ is a scalar controller that will be zero, if the energy tank is depleted ($S \le 0$) and the tracker needs more energy from the energy tank for active control action ($Z \ge 0$), or if the energy tank is full ($S \ge \bar{S}$) and the tracker is passive in interaction and charging the tank with more energy ($Z > 0$). Now the scalar function $\gamma(Z,S)$ in (22) is set to produce controlling

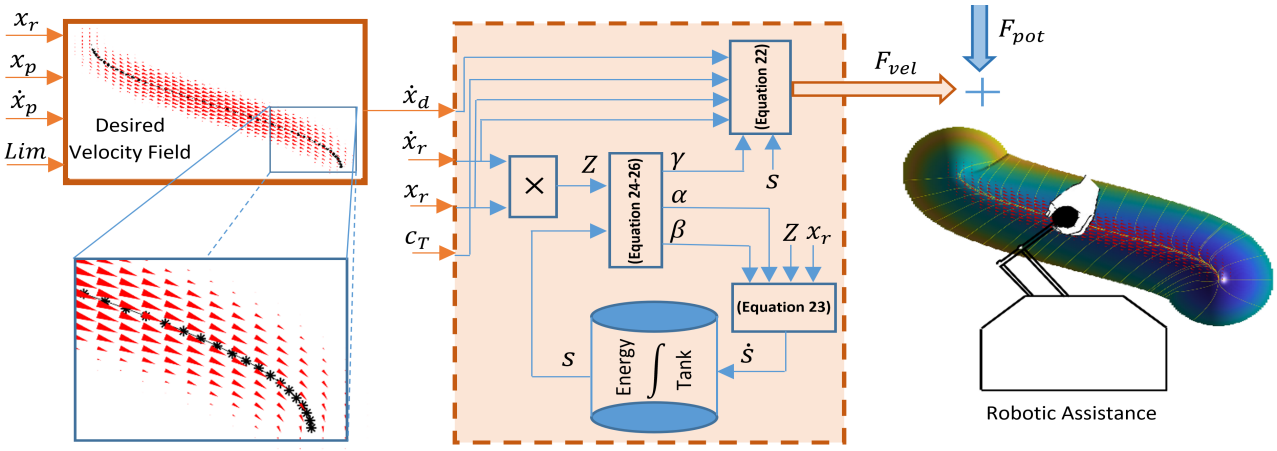

Fig. 4. The proposed velocity field controller. In each position (x_r), the desired velocity is calculated from the demonstrated velocity (x_p, $\dot{x}_p$), then forwarded to the variable dissipative field controller with the energy tank to be followed passively. Finally, the force produced by the velocity field controller (F_{vel}) is added to the force produced by the potential field function (F_{pot}) to provide assistance to the patient to accomplish the task.

action when energy tank is depleted as:

$$\gamma(Z,S) = \begin{cases} 1 & \text{if } S \geq \overline{S} \ \& \ Z \leq 0 \\ \beta(Z,S) & \text{otherwise} \end{cases} \tag{26}$$

Note that the parameter $\gamma(Z,S)$ is different from $\beta(Z,S)$ where the tracking action is passive ($Z \leq 0$) but the energy tank is full ($S \geq \overline{S}$) and therefore, additional dissipated energy is discarded. Fig. 4 displays the overall framework for reproduction of motion with a velocity field controller.

Having both the potential field and velocity field controller with its energy tank stabilizer, the stability of the proposed framework can be investigated. Let us define a candidate Lyapunov function as:

$$\nu(x_r,\dot{x}_r) = \frac{1}{2}\dot{x}_r^T M \dot{x}_r + U(x_r) + S \tag{27}$$

which consists of the kinetic, potential, and tank energy in the system, respectively. The proposed energy function $\nu(x_r,\dot{x}_r)$ is a positive definite function based on (1), (8), and (23). The time derivative of $\nu(x_r,\dot{x}_r)$ is:

$$\dot{\nu}(x_r,\dot{x}_r) = \dot{x}_r^T M \ddot{x}_r + \frac{1}{2}\dot{x}_r^T \dot{M} \dot{x}_r + \dot{x}_r^T \nabla U(x_r) + \dot{S}. \tag{28}$$

Finding $M\ddot{x}_r$ by rearrangement of robot dynamic (1), replacing the equivalent control force (F_C) from (5), (6), and (22) and substituting $\dot{S}$ from (23), yields:

$$\begin{aligned} \dot{\nu}(x_r,\dot{x}_r) = \dot{x}_r^T [&F_{pa} + F_d - \nabla U(x_r) - D(x_r)\dot{x}_r \\ &+ \gamma(Z,S) c_T \dot{x}_d(x_r) - C(x_r,\dot{x}_r)\dot{x}_r - G(x_r) - f(\dot{x}_r)] \\ &+ \frac{1}{2}\dot{x}_r^T \dot{M} \dot{x}_r + \dot{x}_r^T \nabla U(x_r) + \alpha(S)\dot{x}(x_r) D(x_r) \dot{x}(x_r) \\ &- \beta(Z,S) c_T \dot{x}(x_r)^T \dot{x}(x_d). \end{aligned} \tag{29}$$

Rearranging the terms and considering the skew symmetric property of $\dot{M} - 2C(x_r,\dot{x}_r)$, (29) is simplified to (30). Considering that the scalar functions α, β, and γ satisfy the conditions (24), (25), and (26), respectively, the term $\eta(x_r,\dot{x}_r,Z,S)$ in (30) is guaranteed to be positive. Based on the passivity criteria defined in [19], with a lower bounded energy function (27), the rate of change in energy ($\dot{\nu}$) is smaller than the inserted energy ($\dot{x}_r^T[F_{pa}+F_d]$), therefore the system is passive.

$$\begin{aligned} \dot{\nu}(x_r,\dot{x}_r) &= \dot{x}_r^T [F_{pa} + F_d] - [1-\alpha(S)]\dot{x}_r^T D(x_r)\dot{x}_r \\ &\quad + [\gamma(Z,S) - \beta(Z,S)] c_T Z - \dot{x}_r^T f(\dot{x}_r) \\ &= \dot{x}_r^T [F_{pa} + F_d] - \eta(x_r,\dot{x}_r,Z,S) \\ &\leq \dot{x}_r^T [F_{pa} + F_d] \end{aligned} \tag{30}$$

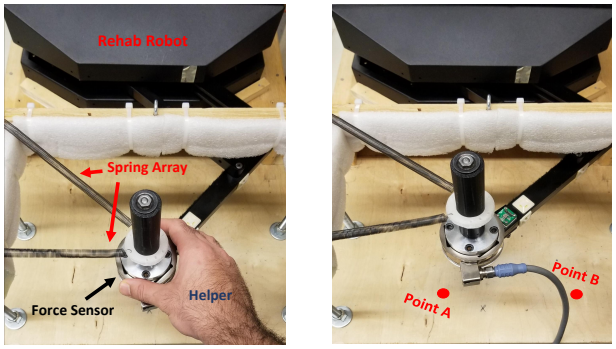

(a) Demonstration phase (b) Robotic assistance phase

Fig. 5. This figure depicts the experiment setup for experiment 1 in both (a) demonstration and (b) robotic assistance phases. Spring array is used for simulation of spastic symptoms of CP.

V. Experimental Evaluation

The proposed framework is experimentally evaluated using a Quanser rehabilitation robot (Quanser Consulting Inc., Markham, Canada). A force sensor (Gamma SI-32-2.5, from ATI Inc, Goodworth, NC, USA) was connected to the end-effector in order to measure the interaction force applied by the therapist to patient's hand as shown in Fig. 5. The parameters used in the system are brought in Table I. Three different scenarios have been considered to evaluate the performance of the proposed potential and velocity field

controllers in the point-to-point position and impedance-based motions. Most of the daily tasks can be decomposed into point-to-point motion or impedance-based primitives. The main symptoms of cerebral palsy, i.e., stiffness in joints and muscles and incoordination is first simulated by spring arrays to assess the capability of the system under passive interaction condition. Then, the system is evaluated in an experiment with an individual with CP.

TABLE I
THE SELECTED SYSTEM PARAMETERS FOR EXPERIMENTS

$K_{min} = 200$	Minimum stiffness parameter
$K_{max} = 600$	Maximum stiffness parameter
$\sigma = 0.02\ m$	Smoothing parameter
$\overline{S} = 20\ J$	Energy capacity in the tank
$L = 0.03\ m$	Width of the velocity field
$c_N = 20\ N.sec/m$	Normal damping parameter
$c_T = 20\ N.sec/m$	Tangential damping parameter
$c_{env,1} = 20\ N.sec/m$	Environment damping
$c_{env,2} = 0\ N.sec/m$	Environment damping

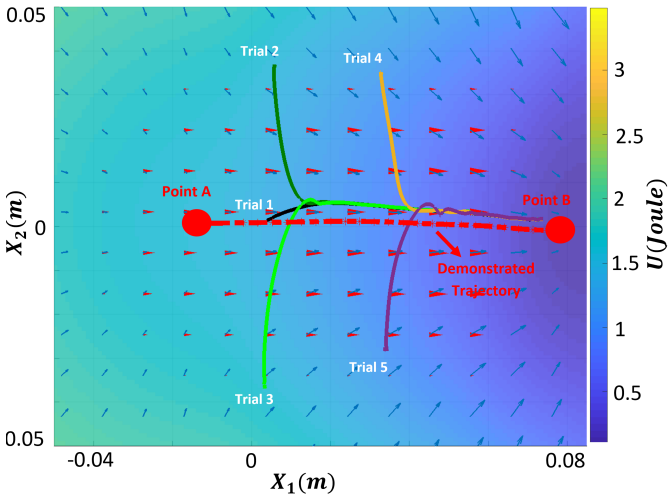

Fig. 6. The learned potential field function in Experiment 1. The blue scale gives the magnitude (the darker, the lower the potential). Arrows indicate the direction of the force in each position. The red line is the demonstrated trajectory by the therapist. The red arrows (triangles) demonstrate the velocity field along the trajectory. As seen in this figure, in all five trials, the potential field attracts the robotic manipulator to the trajectory and then to point B.

A. Simulation of CP symptoms using spring arrays

Spring arrays were used as a systematic way to reproduce same interaction behaviour and evaluate the performance of the system with different parameters. Also, the spring array can roughly represent a passive user with disability to introduce stiffness in interaction dynamics (muscles stiffness) and in-coordination (equilibrium point can be different with the destination). For the first experiment, a 2-dimensional point-to-point motion was used. As shown in Fig. 5, the springs will represent a patient with stiff muscles. The patient is expected to move the robotic end effector from the starting point A to the target point B directly. As seen in Fig. 5, the spring array equilibrium point was close to point A, therefore the task could not be completed without robotic assistance. Thus, a helper (the first author in this work) demonstrated the desired trajectory between points A and B by dragging the robot end-effector to point B. Then, using the system parameters from Table I, the potential and velocity fields were learned as displayed in Fig. 6 to replicate the helper's demonstrated trajectory (i.e., position, velocity, and interaction force). Note that the demonstrated velocity is set to zero for attracting points close to the target, point B, to prevent overshooting the target point and increase the safety of the system. The same strategy has been executed for all the experiments hereafter. Next, in the therapist's absence, using the potential field function gradient (6) and velocity field controller (22), the robotic assistance was provided to the spring array in five trials. In these trials, the robot's end effector was released in five different locations to highlight the convergence of the model and evaluate its performance in replicating the demonstrated velocity and interaction force.

As illustrated in Fig. 6, in all the trials the model successfully attracted the robotic manipulator toward point B. However, since the spring array exerted a force in $-X_1$ and X_2 directions, it can be observed that the robotic manipulator deviated from the demonstrated trajectory in those directions. The level of deviation from the demonstrated trajectory could be controlled by tuning K_{min} and K_{max} parameters. The higher these stiffness parameters, the lower the deviation from demonstrated trajectory (i.e., lower freedom and contribution from the patient in the task execution).

Fig. 7(a) shows the velocity in X_1 direction in demonstration phase in all the five trials. Since the controller is time-independent, the tracking performance is analyzed spatially. In this experiment, we provided high damping behavior in the environment (Table I) to further evaluate the robustness of the controller. This damping behavior in the task environment was not present in the demonstration phase, therefore the learned interaction force captured in the potential field falls short to accelerate the robot enough to reach the demonstrated velocity. As showed in Fig. 7(a), due to the static friction of the system and transient response of the controller, the robot slowly converged to the demonstrated velocity and compensated for force perturbations. At the end of the trajectory, the desired velocity field was set to zero to prevent a shift from the convergence point of the potential field. Therefore, the velocity suddenly decreases to zero (velocity field works as a brake).

The potential field is learned to provide the same interaction force in the tangential direction as in the demonstration phase along the trajectory. Fig. 7(c) shows the interaction force exerted by the potential field (F_{pot}) in X_1 direction which is identical to the demonstrated interaction force as soon as the robot is attracted to the vicinity of the trajectory.

The velocity field controller F_{vel}, as illustrated in Fig. 7(b), mainly exerts assistive force in the same direction as of the

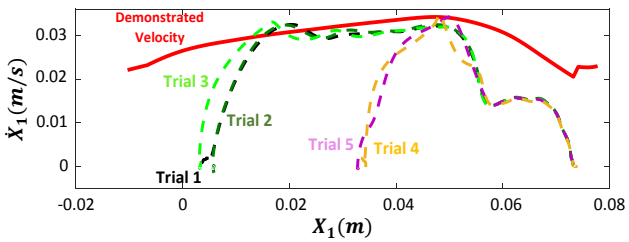

(a) Velocity

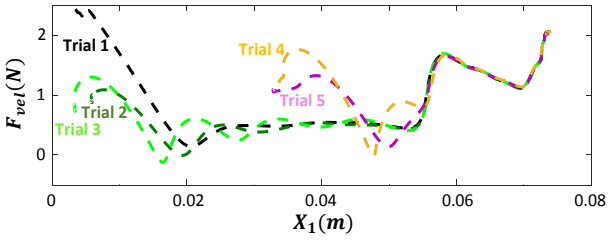

(b) Velocity field controller

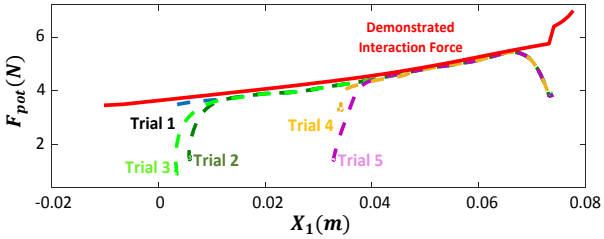

(c) Potential field function force

Fig. 7. (a) Depicts the velocity tracking for Experiment 1, with the vertical and horizontal axis representing the position and velocity in X_1 direction. As observed, the system assists the spring array to reach the desired velocity in each position (as demonstrated by red colour). (b) Depicts the force produced by the velocity field controller F_{vel}. (c) Illustrates the interaction force by the potential field function F_{pot} in X_1 direction. As soon as the robotic manipulator is attracted to the trajectory, the potential field function exerts an interaction force identical to the demonstration phase (red plot).

motion to compensate the damping in the environment. At points A and B, the velocity field controller compensated for the inertia and static friction in the system. Also, at the end of the motion, F_{vel} increased to compensate for the drop in the F_{pot}.

In experiment 2, the aim is to demonstrate how the velocity controller can be tuned to limit patient's deviation from the demonstrated velocity. As shown in Fig. 8, the task consisted of moving a ring attached to the robot's handle along a curved wire without touching the latter. The game would be completed successfully if the patient could move the ring from point A to point B, without any direct contact between the ring and the wire.

The robot equilibrium point was close to point A. Since springs are used to simulate the patient, the task could not be performed without robotic assistance. Thus, in the demonstration phase, the helper grabbed the robot end effector and moved it to point B, and end effector's position, velocity and interaction force data were captured as shown in Fig.

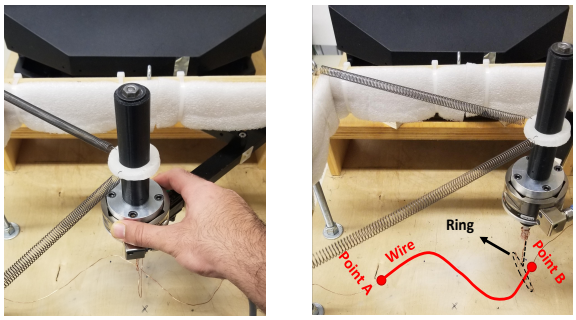

(a) Demonstration phase (b) Robotic assistance phase

Fig. 8. This figure depicts the experiment setup for experiment 2 in both (a) demonstration phase and (b) robotic assistance phase.

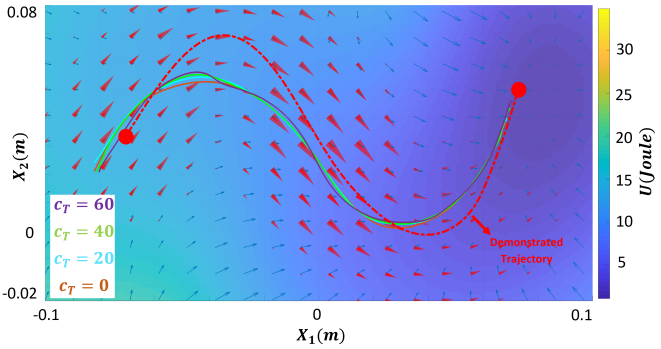

Fig. 9. Depicts the velocity field and learned potential field around the demonstrated trajectory from point A to point B in experiment 2. The system successfully assisted the spring array to move the ring through the wire from point A to point B without hitting the wire in all 4 trials with different c_T parameter.

9. Finally, in the robotic assistance phase, the task was performed successfully with robotic assistance in all four performed trials. No damping was added to the environment. Because of the deviation of the spring array from the demonstrated trajectory, the interaction force to the robotic manipulator was higher Compared to the demonstrated phase (The potential field attracts the robot toward trajectory). Also, higher velocities at the end of the trajectory was observed as it was expected, Fig. 10(a) with $c_T = 0$. c_T parameter in (19-21) represents the velocity tracking gain in tangential direction. In order to evaluate the performance of velocity field controller in velocity regulation with its c_T parameter in each trial, a different value for c_T was assigned. As illustrated in Fig. 10, the higher the c_T parameter, the higher the control force from the velocity field controller and the lower the deviation from the demonstrated velocity. However, with higher c_T parameter, the more the oscillatory behavior in the transient response. Therefore, c_T should be tuned based on the specific robotic system and application.

Fig. 10(a) and Fig. 10(b) show that when the robotic manipulator was going slower than the demonstrated velocity, the velocity field controller exerted an assistive force in the direction of the motion. On the other hand, when the robot was moving faster than the desired velocity, the robot resisted the motion. In Fig. 11 with $c_T = 0$ (no velocity tracking

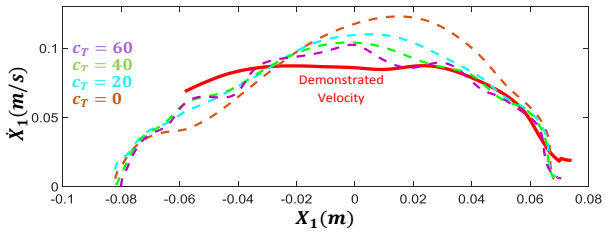

(a) Velocity in X_1

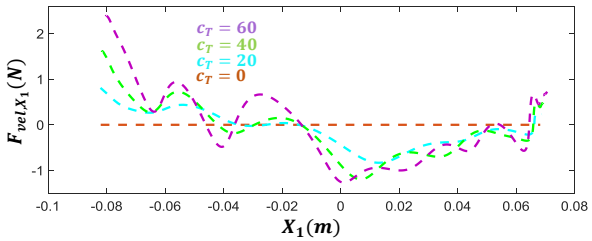

(b) Velocity field controller force in X_1

Fig. 10. (a) Depicts the observed velocity tracking in X_1 direction in all four trials with different c_T in experiment 2, respectively. As seen, the velocity tracking of demonstrated velocity (red plot) gets more accurate as the c_T parameter increases . (b) Shows the control signal produced by velocity field controller F_{vel} in X_1 direction for each trial, respectively. F_{vel} increases as the c_T parameter increases.

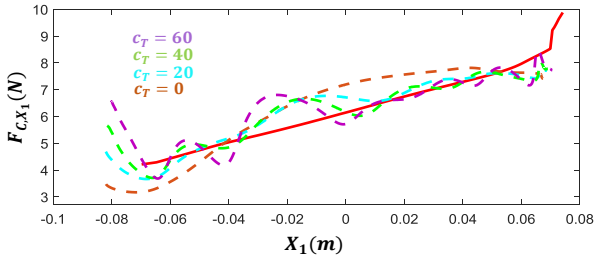

Fig. 11. This figure shows the demonstrated interaction force (red plot) and the observed control signal (F_C) in X_1 direction that is the sum of potential field (F_{pot}) and velocity field (F_{vel}) forces. As observed, the velocity field compensates for the environment disturbance and difference between the potential field force and the demonstrated (required) interaction force. The more the c_T parameter is, the better the compensation will be (however oscillatory behaviour increased due to the system dynamics).

in tangential direction) due to the modelling error in the potential field and robot deviation from the trajectory the interaction force is slightly different from the demonstrated interaction force from the therapist. Fig. 11 shows how the velocity field controller compensates for this difference.

B. Experiment with an individual with CP

A single-case study was conducted with a 51 years old female individual with quadriplegic CP (called user hereafter in the experiments). She has a mixed CP condition characterized by high and low muscle tone and high involuntary movements. Based on the Manual Ability Classification System (MACS), she is at Level III, meaning she has difficulty handling objects by hand but is able to perform manual tasks with assistance and/or adaptation of the activity [20].

(a) Demonstration phase

(b) Robotic assistance phase

Fig. 12. Depicts the experiment setup for experiment 3 with an individual with CP (a) demonstration phase. (b) robotic assistance phases.

A designed 2-dimensional virtual game was projected on an LCD screen, placed in front of the user. The user was asked to move a cursor on the screen with the robotic manipulator toward the destination point, point A, by passing through 2 gaps with different directions without hitting them, Fig. 13. This experiment was challenging for the user as it needed high levels of muscle control and coordination. This experiment aimed to evaluate the system under realistic condition in interaction with an individual with CP to assess the overall performance and stability of the system. Fig. 12 illustrates the experimental setup in the demonstration and robotic assistance phases. Also parameters in table I was used for this experiments. In the demonstration phase, first the helper assisted the user in a single task execution to complete the task successfully. Then, the potential and velocity fields that were learned from the demonstrated performance were used to assist the user.

Fig. 13 shows the results for this experiment in three trials, each column represents results for each trial. First column shows the result for user trial with no assistance provided in three tryouts, Fig. 13(a). As illustrated with the uncoordinated and involuntarily movements, the user could not control the robotic manipulator and was unable to complete the task successfully and was not passing exactly through the gaps on LCD. Then the helper assisted the user to complete the task successfully, Fig. 12(a). With the demonstrated performance, the system learned to replicate the helper's assistance.

In the second trial (Fig. 13(b)), the user performed the task again with learned potential field and no velocity field ($c_T = 0$). The user could successfully complete the task in three tryouts without hitting any of the gaps. The potential field was restricting the user motion in normal direction, also the user was moving consistently toward the destination due to the tangential force (slope) in the potential field. Even though the normal force-tracking is close to the demonstrated normal force by the helper (due to the high K parameter, $K = K_{max}$), the velocity tracking was poor and variations in task completion time by user were observed (not consistent with duration in demonstration phase).

In the third trial (Fig. 13(c)), velocity field was also added based on the helper's velocity in demonstration phase and potential field was tuned to be weaker ($K = K_{min}$). It was

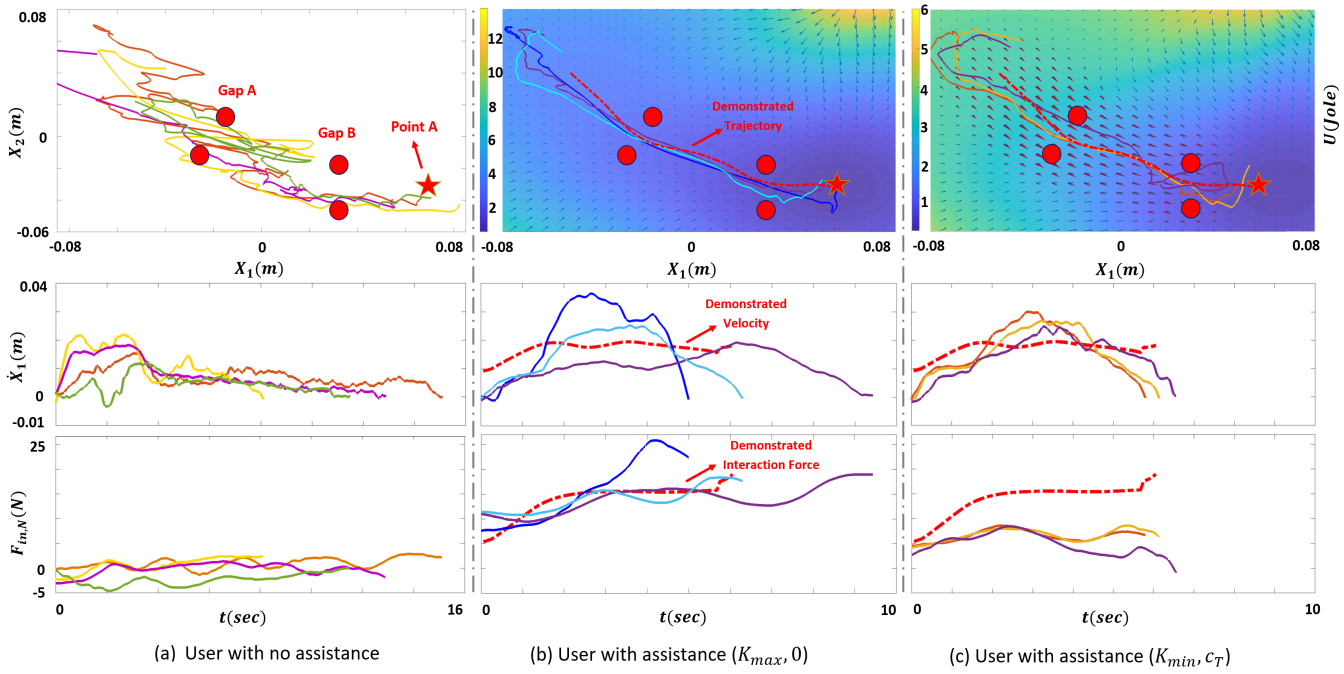

Fig. 13. This figure shows the results from a user with CP completing the task of moving a cursor on LCD screen (controlled with robotic manipulator) toward a destination point (red star) through gaps A and B (red circles) without hitting them, in three trials . Row one, two and three in the figure depicts the position (X_1 - X_2), velocity in X_1 direction (X_1 - t) and normal interaction force ($F_{in,N}$ - t) for each trial, respectively. (a) Trial results of the user with no assistance provided from a helper/robotic manipulator. (b) Trial results with robotic assistance with potential field and no velocity field ($K = K_{max}$ and $c_T = 0$) in three tryouts. (c) Trial results with robotic assistance with velocity field and a lower magnitude potential field ($K = K_{min}$ and c_T) in three tryouts.

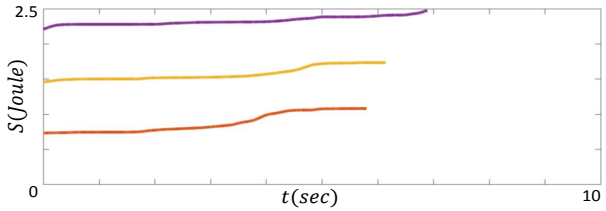

Fig. 14. Shows the energy tank state (S) in each of the tryouts in Fig. 13(c). The energy tank is slowly charging up overtime due to the active interaction with the user in these tryouts.

apparent that we had good velocity tracking and timing but weaker force tracking in normal direction. In one of the tryouts (violet trajectory) the user failed to pass through gap A and B due to the weaker potential field with less assistance in normal direction.

The velocity field controller with its energy tank mechanism ensured the stability and passivity of the overall system in third trial, Fig. 13(c). The velocity field controller damped the patient's active energy in the normal direction and saved it up in the energy tank state S as shown in Fig. 14. At the same time, it used the stored energy to actively regulate the deviation of the patient based on the demonstrated velocity along the trajectory.

C. Discussion

The proposed framework has merits in rehabilitation and assistive technologies to replicate the therapist's short intervention in point-to-point trajectory-following motion tasks. Only one demonstration is required, which helps the therapist to save time and effort. However, the system needs to be robust to inevitable noise and uncertainty in both the learning and reproduction phases. The demonstrated data is first low pass filtered temporally; then, Gaussian kernels smooth out the generalized fields spatially to prevent sharp bumps or edges. Also, in the reproduction phase, the proposed performance-based velocity field controller provides adaptive assistance to compensate for the variable user performance and environment distortions. Still, if the patient's behavior is highly non-consistent, one can easily average (temporally or spatially) through multiple demonstrations and then teach the proposed system based on the averaged demonstration.

The velocity field only exists in the vicinity of the trajectory in the direction toward the destination point and converges to zero as you get far from it. Therefore, the proposed velocity field controller damps (resists) motions that are diverging from both the trajectory and destination point. Also, having the energy tank mechanism to ensure the passivity of this active controller makes the system appropriate for the target application in this paper that requires high safety standards. However, in theory, the joined potential and velocity fields may not be globally asymptotically stable around the destination point and there might be local minima (converging points) usually in areas far from the trajectory when there is a sharp turn. This can be solved by tuning the width of the velocity field and setting the desired velocity to zero close to the target destination to minimize the possible interference.

Recently, other research groups are getting interested in applying LfD in rehabilitation and assistive robotics. [21] has used dynamic motion primitive to adapt and generalize a trajectory-following motion to the user's motion style. The main difference between the proposed system and [21] is that the potential and velocity fields also explicitly encapsulate and generalize interaction force, velocity and interaction impedance (stiffness and damping) of the demonstrated trajectory. This is the contribution of this system which results in a generalized, natural-looking, and safe reproduction of therapist assistance. The proposed system, with the use of energy tank state is also proven to be passive and stable which is critical in applications involving interaction with individuals with disability. Furthermore, unless our previous work [11]–[14], this system is position indexed and generalizes therapist demonstrated assistance to provide appropriate force at any point in the workspace towards the destination. It also accounts for interaction force with both therapist and patient being involved in the demonstration phase.

However, the proposed system is somewhat task-specific and requires demonstrations from the therapist if the task changes in the environment. In the future, the main focus of our work will be to 1) develop a reinforcement learning algorithm to update the potential field based on user performance in task execution, 2) develop an algorithm to generalize the therapist's demonstrated assistance in the task environment and learn the required potential and velocity fields for any point-to-point motion in that environment without the need for a therapist's demonstration, and 3) perform more experiments with more individuals with disability (Stroke, CP) to clinically analyze the system.

VI. Conclusion

The proposed learning from demonstration framework for robotic assistance can have applications in various tasks that involve cooperative human-robot task execution. Without the loss of generality, an application for assist-as-needed assistance to people with disability was the primary focus of this paper. The framework, with its potential field function and velocity field controller, was modified and developed to reproduce and generalize the helper's assistance (i.e., trajectory, velocity, interaction force) with only a single demonstration. The efficacy and performance of the system were evaluated in three scenarios involving spring arrays for systematic analysis of system performance and an individual with CP.

References

[1] N. Paneth, T. Hong, and S. Korzeniewski, "The descriptive epidemiology of cerebral palsy," *Clinics in perinatology*, vol. 33, no. 2, pp. 251–267, 2006.

[2] H. Krueger, J. Koot, R. E. Hall, C. O'callaghan, M. Bayley, and D. Corbett, "Prevalence of individuals experiencing the effects of stroke in canada," *Stroke*, vol. 46, no. 8, pp. 2226–2231, 2015.

[3] A. Ríos-Rincón, K. Adams, J. Magill-Evans, and A. Cook, "Playfulness in children with limited motor abilities when using a robot," *Physical & Occupational Therapy in Pediatrics*, vol. 36, no. 3, pp. 232–246, 2016.

[4] H. van der Ploeg, A. van der Beek, L. van der Woude, and W. van Mechelen, "Physical activity for people with a disability," *Sports Medicine*, vol. 34, no. 10, pp. 639–649, 2004.

[5] H. I. Krebs, J. J. Palazzolo, L. Dipietro, M. Ferraro, J. Krol, K. Rannekleiv, B. Volpe, and N. Hogan, "Rehabilitation robotics: Performance-based progressive robot-assisted therapy," *Autonomous robots*, vol. 15, no. 1, pp. 7–20, 2003.

[6] S. K. Campbell, R. J. Palisano, and D. W. V. Linden, *Physical Therapy for Children*. Elsevier Saunders, 2006.

[7] W. H. Chang and Y. H. Kim, "Robot-assisted therapy in stroke rehabilitation," *Journal of stroke*, p. 174–181, 2013.

[8] F. Ferraguti, C. Secchi, and C. Fantuzzi, "A tank-based approach to impedance control with variable stiffness," in *IEEE International Conference on Robotics and Automation*. IEEE, 2013, pp. 4948–4953.

[9] S. Chernova and A. Thomaz, "Robot learning from human teachers," *Synthesis Lectures on Artificial Intelligence and Machine Learning*, vol. 8, no. 3, pp. 1–121, 2014.

[10] B. Argall, S. Chernova, M. Veloso, and B. Browning, "A survey of robot learning from demonstration," *Robotics and autonomous systems*, vol. 57, no. 5, pp. 469–483, 2009.

[11] M. Najafi, M. Sharifi, K. Adams, and M. Tavakoli, "Robotic assistance for children with cerebral palsy based on learning from tele-cooperative demonstration," *International Journal of Intelligent Robotics and Applications*, pp. 1–12, 2017.

[12] M. Najafi, K. Adams, and M. Tavakoli, "Robotic learning from demonstration of therapist's time-varying assistance to a patient in trajectory-following tasks," in *International Conference on Rehabilitation Robotics (ICORR)*. IEEE, 2017.

[13] M. Maaref, A. Rezazadeh, K. Shamaei, and M. Tavakoli, "A gaussian mixture framework for co-operative rehabilitation therapy in assistive impedance-based tasks," *IEEE Journal of Selected Topics in Signal Processing*, vol. 10, no. 5, pp. 904–913, Aug 2016.

[14] M. Maaref, A. Rezazadeh, K. Shamaei, R. Ocampo, and T. Mahdi, "A bicycle cranking model for assist-as-needed robotic rehabilitation therapy using learning from demonstration," *IEEE Robotics and Automation Letters*, vol. 1, no. 2, pp. 653–660, July 2016.

[15] S. M. Khansari-Zadeh and O. Khatib, "Learning potential functions from human demonstrations with encapsulated dynamic and compliant behaviors," *Autonomous Robots*, vol. 41, no. 1, pp. 45–69, 2017.

[16] k. Kronander and A. Billard, "Passive interaction control with dynamical systems," *IEEE Robotics and Automation Letters*, vol. 1, no. 1, pp. 106–113, 2016.

[17] N. Chia Bejarano, S. Maggioni, L. De Rijcke, C. Cifuentes G., and D. J. Reinkensmeyer, *Robot-Assisted Rehabilitation Therapy: Recovery Mechanisms and Their Implications for Machine Design*, 01 2016, vol. 10.

[18] C. Rossa, M. Najafi, M. Tavakoli, and K. Adams, "Nonlinear workspace mapping for telerobotic assistance of upper limb in patients with severe movement disorders," in *2017 IEEE International Conference on Systems, Man, and Cybernetics (SMC)*, Oct 2017.

[19] J. Slotine and W. Li, *Applied Nonlinear Control*. Prentice Hall, 1991.

[20] N. Jafari, K. Adams, M. Tavakoli, and a. H. J. Sandra Wiebe, "Usability testing of a developed assistive robotic system with virtual assistance for individuals with cerebral palsy: a case study," *Journal of Disability and Rehabilitation- Assistive Technology*, 2017.

[21] E. G. C. Lauretti, F. Cordella and L. Zollo, "Learning by demonstration for planning activities of daily living in rehabilitation and assistive robotics," *IEEE Robotics and Automation Letters*, pp. 1375–1382, 2017.

Mohammad Najafi is a Machine Learning Engineer at XSENSOR Technology Corporation in Calgary, AB, Canada. He was a research associate at Telerobotic and Biorobotic Systems Laboratory, University of Alberta, Edmonton, AB, Canada and received his MSc degree at the School of Electrical and Computer Engineering at the University of Alberta, in 2018. He also pursued his BSc degrees in electrical engineering (control systems and communications) from Amirkabir University of Technology, Tehran, Iran, in 2015. His research interests are medical robotics, machine learning, robot learning from demonstration, assistive technology, human-robot interaction and haptics.

Carlos Rossa is an Assistant Professor of Mechatronics in the Faculty of Engineering and Applied Science at the Univerity of Ontario Institute of Technology, Oshawa, ON, Canada. He received his BEng and MSc degrees in Mechanical Engineering from the Ecole Nationale d'Ingenieurs de Metz, Metz, France, both in 2010, and earned his PhD degree in Mechatronics and Robotics from the Universite Pierre et Marie Curie, Paris, France, in 2013, under the auspices of the French Atomic Energy Commission (CEA). From 2014 to 2017, he was a post-doctoral fellow at the University of Alberta, Edmonton, Canada. His research interests include medical robotics, haptics, and mechatronics.

Kim Adams is an Associate Professor with the Faculty of Rehabilitation Medicine at the University of Alberta, Edmonton, AB, Canada, and a Research Affiliate with the Glenrose Rehabilitation Hospital. She received her PhD degree in Rehabilitation Science from the University of Alberta, Canada, in 2011. Dr. Adams's professional interests are assistive technology design, development and evaluation, use of assistive robots for children with physical disabilities to engage in play and learning activities, Human factors engineering, augmentative and alternative communication.

Mahdi Tavakoli is a Professor with the Department of Electrical and Computer Engineering, University of Alberta, Edmonton, AB, Canada. He received the Ph.D. degree in electrical and computer engineering from the University of Western Ontario, London, ON, Canada, in 2005. In 2006, he was a Postdoctoral Researcher at Canadian Surgical Technologies and Advanced Robotics. In 2007-2008, he was a Natural Sciences and Engineering Research Council Postdoctoral Fellow with Harvard University, Cambridge, MA, USA. His research interests broadly include the areas of robotics and systems control. Dr. Tavakoli is currently on the Editorial Board of the IEEE/ASME Transactions on Mechatronics.